International Journal of Nanomedicine

Dovepress
open access to scientific and medical research

Open Access Full Text Article

ORIGINAL RESEARCH

Shape-dependent antibacterial effects of non-cytotoxic gold nanoparticles

This article was published in the following Dove Press journal:
International Journal of Nanomedicine
29 March 2017
Number of times this article has been viewed

Jelle Penders[1,2]
Michelle Stolzoff[3]
Daniel J Hickey[1]
Martin Andersson[2]
Thomas J Webster[1]

[1]Department of Chemical Engineering, Northeastern University, Boston, MA, USA; [2]Department of Chemistry and Chemical Engineering, Chalmers University of Technology, Göteborg, Sweden; [3]Department of Bioengineering, Northeastern University, Boston, MA, USA

Abstract: Gold nanoparticles (AuNPs) of various shapes (including spheres, stars and flowers), with similar dimensions, were synthesized and evaluated for their antibacterial effects toward *Staphylococcus aureus*, a bacterium responsible for numerous life-threatening infections worldwide. Optical growth curve measurements and Gompertz modeling showed significant AuNP shape- and concentration-dependent decreases in bacterial growth with increases in bacterial growth lag time. To evaluate prospective use in in vivo systems, the cytotoxicity of the same AuNPs was evaluated toward human dermal fibroblasts in vitro by 3-(4,5 dimethylthiazol-2-yl)-5-(3-carboxymethoxyphenyl)-2-(4-sulfophenyl)-2H-tetrazolium (MTS) viability assays and confocal microscopy. No indication of any mammalian cell toxicity or morphological effects was found. Additionally, it was observed that the AuNPs were readily internalized in fibroblasts after 4 days of incubation. Most importantly, the results of the present study showed that gold nanoflowers in particular possessed the most promising non-cytotoxic mammalian cell behavior with the greatest shape-dependent antibacterial activity-promising properties for their future investigation in a wide range of anti-infection applications.

Keywords: gold, nanoparticles, nanoflowers, nanostars, *S. aureus*, fibroblasts

Video abstract

Point your SmartPhone at the code above. If you have a QR code reader the video abstract will appear. Or use:

http://youtu.be/EvqAmrIkVIs

Correspondence: Thomas J Webster
Department of Chemical Engineering, Northeastern University, 360 Huntington Avenue, Boston, MA 02115, USA
Tel +1 617 373 6585
Fax +1 617 373 6555
Email th.webster@neu.edu

Introduction

In the field of nanomaterials, gold nanoparticles (AuNPs) have been shown to exhibit a broad range of interesting shape- and size-dependent properties, vastly different from their bulk counterparts, which allows them to be used for a variety of applications. For example, their enhanced reactivity makes them suitable in catalysis[1] and their strong surface plasmon resonance effects allow for applications in optics.[2] AuNPs have been synthesized in a variety of shapes and sizes, with gold nanospheres (AuNSs) being the most common, made conventionally by an adaptation of the Turkevich method.[3] Notable changes in AuNP morphology have been achieved through the addition of certain surfactants, resulting in gold nano-rods,[4,5] cubes[6] and stars.[7]

More recently, AuNPs have been hallmarked as a very promising material for biological applications.[8] Several researchers are investigating ways to utilize their properties for biosensors,[9] as vessels for drug delivery[10] and even to selectively treat cancer cells.[11] A promising method for the use of AuNPs in cancer treatment is by inducing hyperthermia, utilizing the photoinduced surface plasmon resonance effect.[12,13] Additionally, AuNPs may be used as a novel antibacterial agent.[14] In particular, relatively few studies have been performed on the antibacterial properties of AuNPs compared to the extensive research on anti-microbial silver nanoparticles (NPs).[15] When the antibacterial effects of AuNPs have been studied, it is mostly in combination with antibacterial surface modifications[16–18] and in conjunction with drugs.[19–22]

submit your manuscript | www.dovepress.com
Dovepress
http://dx.doi.org/10.2147/IJN.S124442

The goal of using antibacterial NPs, and the focus of this work, is to aid in the treatment of increasingly antibiotic-resistant infections. Antibiotic-resistant bacterial strains, including methicillin-resistant *Staphylococcus aureus* (MRSA), pose severe threats to humanity[23] and are recurrent in hospitals worldwide.[24,25] Antibacterial NPs could bypass the increasing rates of antibiotic resistance by attacking and destroying the bacteria in other ways, including induced hyperthermia, a method similar to their proposed anti-cancer applications.[26,27] Another possibility investigated here is the induction of an antibacterial effect via morphological interactions, via sharp edges or protrusions with a high aspect ratio, which could potentially pierce and rupture the bacterial membrane. Most research on morphological interactions has been performed on micro- and nano-patterned surfaces,[28,29] where surfaces with a high aspect ratio, spikes or pillars have been shown to reduce bacterial colonization and induce bacterial lysis due to high local stresses on the bacterial cell wall.[30,31] Other physical anti-bacterial methods have recently been shown, based on disrupting the bacterial membrane utilizing magnetic NPs in combination with radiofrequency current or bimetallic NPs, to induce a loss of bacterial membrane potential.[32,33] These strategies, belonging to the emerging field of nanomedicine, show the possibility of ridding humanity of some of its biggest bacterial threats and could help save the lives of millions.

However, a word of caution is necessary regarding the potential use of NPs in vivo since an apparent cytotoxicity of some NPs toward healthy cells has raised concerns.[27,34,35] As with all NPs, AuNPs have varying degrees of cytotoxicity, which is dependent on their size,[36–38] surface chemistry,[35,39–41] shape[34,42,43] and most importantly dosage.[18] Various trends in size-dependent cytotoxicity have been observed, most commonly showing an increased cytotoxicity for smaller sized NPs, particularly those <5 nm.[38] The surface chemistry of NPs also highly influences apparent cytotoxicity, showing concentration-dependent cytotoxicity for often-used citrate-capped AuNS.[34] Additionally, the presence of unreacted citrate and Au^{3+} ions can induce photomutagenic effects by the formation of free radicals.[44] The shape of the AuNPs can also significantly influence cytotoxicity and uptake efficacies, showing a decreased cytotoxicity for rods over spherical particles and increased uptake into cells.[34] Therefore, in conjunction with measuring efficacy via antibacterial assays, a thorough cytotoxicity evaluation of any NP is a necessity and a comparison of particles should only be completed on a single factor basis, be it size, shape or surface chemistry;[42] only then can one assess the properties that influence cytotoxicity and/or antibacterial properties.

In the present study, three different geometries of AuNPs – AuNSs, gold nanostars (AuNSTs) and gold nanoflowers (AuNFs) – were synthesized by optimizing recent synthesis methods. The main effort of this optimization was to obtain particles with the same non-cytotoxic surface chemistry and similar dimensions in order to isolate the effects of these unique AuNP shapes. *S. aureus* and human dermal fibroblasts (HDFs) were exposed to solutions of these NPs in varying concentrations, to evaluate shape-dependent antibacterial effects and cytotoxicity. The antibacterial effects were evaluated from continuous optical density (OD) measurements of bacterial growth over 24 hours, after which the data were fitted to the Gompertz model[45] for statistical analysis. Cytotoxicity of the particles toward HDF was evaluated by mitochondrial activity assays (3-(4,5 dimethylthiazol-2-yl)-5-(3-carboxymethoxyphenyl)-2-(4-sulfophenyl)-2H-tetrazolium [MTS]) and cell morphology (confocal microscopy) experiments. HDF cells were chosen as relevant control cells for these assays since *S. aureus* is mainly prevalent as a skin infection.

Materials and methods

NP synthesis

All chemicals were purchased from Sigma-Aldrich (St Louis, MO, USA) and used as received. For all synthesis procedures, ultrapure Milli-Q water (18.2 MΩ) was used as the solvent. A 20 mM $HAuCl_4$ stock solution was prepared by adding 69.2 µL of a 30-wt% solution of $HAuCl_4$ in dilute HCl to 4.9308 mL of Milli-Q water. The solution was kept in darkness at 4°C. The 4-(2-hydroxyethyl)piperazine-1-ethanesulfonic acid (HEPES) buffer solution was prepared by dissolving 0.1 M HEPES buffer in Milli-Q water and bringing the pH of the resulting solution to 7.4 by the addition of 1 M NaOH.

AuNS seeds (~15 nm in diameter) were synthesized according to Park and Park,[46] where 250 µL of 20 mM $HAuCl_4$ was added to 9.75 mL of Milli-Q water and then was brought to boil under continuous stirring. Then, 0.5 mL of a 38.8-mM trisodium citrate solution was added and boiled for 20 min. The solution was cooled down to room temperature under continuous stirring.

The AuNSs were prepared by a modification of the method by Park and Park[46] to obtain spheres ~33 nm in diameter by adding 200 µL of 20 mM $HAuCl_4$ to 8.5 mL Milli-Q water under continuous stirring. Then, 750 µL of AuNS seeds were added, prepared as described earlier, and 1.5 mL of a 5.3 mM ascorbic acid solution was added at 30 µL/min. Stirring continued for at least 30 min after the addition was complete.

AuNSTs were prepared according to Xie et al,[7] by adding 100 µL of 20 mM $HAuCl_4$ to 4 mL of 100 mM HEPES buffer (pH 7.4) and 6 mL of Milli-Q water. The solution was stirred for 30 min until a clear turquoise solution was obtained.

The AuNFs were synthesized according to a modified method by Maiorano et al[47] by adding 500 µL of AuNS seeds, prepared as described earlier, to 2.5 mL of a 100 mM HEPES buffer (pH7.4) and 2.5 mL of Milli-Q water. This solution was placed in an ice bath (~4°C), and 4.17 mL of 1.9 mM $HAuCl_4$ was added at 0.5 mL/min. Stirring continued for at least 30 min after the addition of $HAuCl_4$.

NP purification and quantification

The NP solutions were purified by centrifugation of 10 mL solutions at 7,000 *g* for 10 min. The supernatant was removed and centrifuged again while two pellets were combined with 5 mL of 100 mM of HEPES buffer (pH 7.4). The remaining NPs from the supernatant were added after centrifugation. This procedure was repeated one more time, exchanging any citrate left on the particles with HEPES. For the AuNSs, the solutions were sonicated for 30 min in between steps. Quantification was achieved by lyophilization of the purified NPs solutions overnight and by weighing the solutions before and after this time period. The amount obtained was corrected for the amount of buffer salt present in the solution. The lyophilized samples were resuspended in sterile 100 mM HEPES buffer (pH 7.4) for bacterial studies and complete Dulbecco's Modified Eagle's Medium (DMEM; with 10% fetal bovine serum and 1% penicillin–streptomycin) for cell studies.

Transmission electron microscopy analysis

The NPs were analyzed by transmission electron microscopy (TEM) by placing a drop of the solution on a CF300-Cu TEM grid (Electron Microscopy Sciences, Hatfield, PA, USA) and blotting the excess after 2 min. The grids were analyzed using a JEM-1010 TEM (JEOL, Tokyo, Japan) operated at 80 keV. Various areas on the grids were imaged, and representative images were acquired.

Zeta potential measurements

The zeta potential of the particles was measured using a 90Plus particle size analyzer (Brookhaven Instruments). The particles in DMEM at 1 mg/mL were vortexed for 1 min before measurements and diluted 15 times in 0.1 M HEPES buffer. Measurements were analyzed with the ZetaPALS program using the Smoluchowski method.[48]

Antibacterial studies with *S. aureus*

A culture of *S. aureus* (ATCC 12600) was started the day before each experiment by the inoculation of a single bacterial colony into 5 mL of 3% (wt%) tryptic soy broth (TSB) and grown in a shaking incubator overnight. The cultured bacteria were diluted in 3% TSB to obtain optical density measured at 592 nm (OD_{592})=0.52, which correlates to 10^9 bacteria/mL. The culture was further diluted in TSB and plated at a concentration of 10^6 bacteria/mL. The lyophilized and purified NPs were resuspended in sterile 100 mM HEPES buffer (pH 7.4) to a concentration of 1,000 µg/mL and were further diluted with TSB to 1, 5, 10, 50, 100 and 500 µg/mL solutions. To each well of a 96-well plate, 100 µL of the NP solution was added to 100 µL of a diluted bacteria culture. Each condition was present in triplicate on each plate, and controls with no bacteria were also included. For growth curve measurements, the plate was placed, with lid, in a spectrophotometer (SpectraMax Paradigm; Molecular Devices, Sunnyvale, CA, USA) at 37°C and the OD_{592} was measured over 24 h at 2 min intervals.

Cytotoxicity studies on HDFs

Normal adult HDFs (CC-2511; Lonza, Basel, Switzerland) were cultured in T75 flasks in complete DMEM (with 10% fetal bovine serum and 1% penicillin–streptomycin) and were split by the addition of 5 mL of a 0.05% trypsin solution before use. The cells were centrifuged and resuspended to a concentration of 50,000 cells/mL. The lyophilized and purified NPs were resuspended in complete DMEM and diluted to obtain concentrations of 0.5, 2.5, 5, 25, 50, 250, 500 and 1,000 µg/mL. No phase separation of the NPs upon resuspension in DMEM was observed prior to the addition to the cells. Typically, 100 µL of the cells were seeded in wells of a 96-well tissue culture plate (for a concentration of 5,000 cells/well) and incubated overnight. Subsequently, the medium was removed and 100 µL of the NP solution was added. After 4 days of incubation, an MTS assay was performed by adding a 1:5 (MTS:DMEM) solution to the cells and measuring the absorbance at 490 nm after ~2 h of incubation. The absorbance was also measured immediately after the addition of the MTS solution to correct for the increase in absorbance due to increasing NP concentrations.

Confocal microscopy sample preparation

For this experiment, 18 mm coverslips were pretreated with 5 µg/cm^2 of fibronectin (Corning Cat No 356008) diluted in Ca^{2+}- and Mg^{2+}-free phosphate-buffered saline (PBS). The coverslips were rinsed and placed in the wells of a 12-well

tissue culture plate and then seeded with 12,500 HDF cells/cm^2. The day after, the medium was exchanged and NPs were added. Coverslips were incubated for 4 days, after which the cells were fixed with 4% methanol-free formaldehyde for 10 min and permeabilized in 0.1% Triton X-100 in PBS for 10 min. Non-specific antigens were blocked by incubating overnight in 5% bovine serum albumin (BSA) in PBS at 4°C. Next, the cells were stained for 20 min in succession with fluorescein isothiocyanate (FITC)–anti-vinculin 1:800 in 1% BSA and Alexa Fluor 568 phalloidin 1:20 in 1% BSA in PBS. Additionally, Hoechst 33258 at a 1 µg/mL concentration in Milli-Q water was used to stain the cell nuclei for 5 min. The coverslips were washed in PBS intermittently and after staining and were mounted facedown onto a microscope slide with a drop of mounting solution (SlowFade® Diamond Antifade Mountant; Molecular Probes, Eugene, OR, USA).

Statistical evaluation

All experiments were conducted in triplicate and repeated three times each, including the appropriate controls. Statistics were calculated using a Student's *t*-test, and significance was accepted at $P<0.05$.

Results and discussion

NP synthesis and characterization

Three different shapes of AuNPs were synthesized: AuNSs, AuNSTs and AuNFs. As a precursor for the AuNSs and AuNFs, citrate-stabilized spherical gold seeds were made using a protocol adapted from Park and Park[46] and had a mean diameter of 15.2±1.2 nm. A representative TEM image can be seen in Figure 1A as well as a size distribution and an ultraviolet-visible (UV-VIS) spectrum.

To make the AuNSs, a $HAuCl_4$ solution was added to the Au seeds and further growth was obtained by chemical reduction upon the addition of ascorbic acid. An optimized seed concentration was used to obtain particles with a mean diameter of 33.3±3.8 nm. This synthesis resulted in spherical particles as can be seen in Figure 1B, with the corresponding UV–VIS spectrum and size distribution. The spectrum maximum occurred at 525 nm, which is red shifted 5 nm compared to the seeds. This is expected since the size of the AuNPs and their UV–VIS absorption spectra are directly related.

The AuNSTs were made by a method described by Xie et al[7] by the addition of a $HAuCl_4$ solution to a 100 mM HEPES buffer solution, stabilized at pH 7.4. HEPES

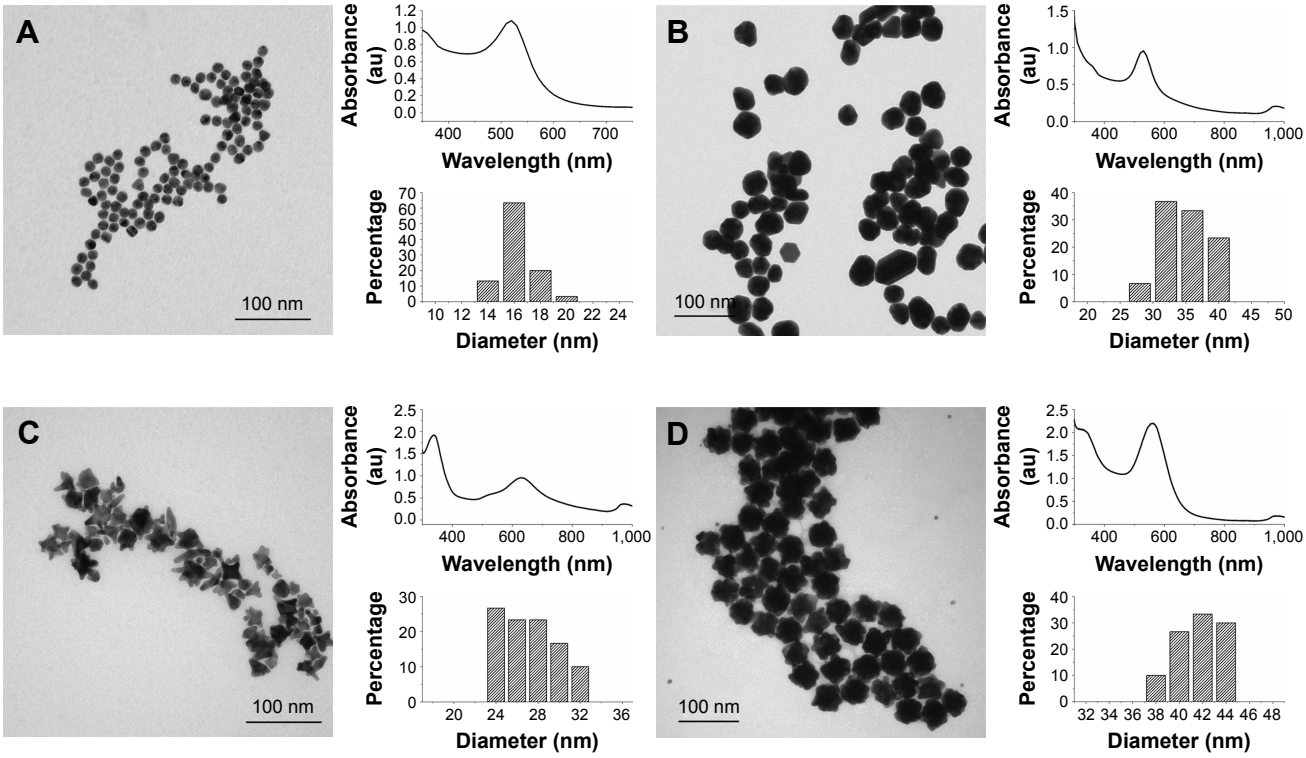

Figure 1 Nanoparticle synthesis and characterization overview of the AuNS seeds, AuNSs, AuNSTs and AuNFs.
Notes: (**A**) AuNS seeds: TEM image of AuNS seeds 15.2±1.2 nm, UV–VIS spectrum with a maximum at 520 nm and a size distribution histogram over 30 measurements. (**B**) AuNSs: TEM image of AuNSs 33.3±3.8 nm, UV–VIS spectrum with a maximum at 525 nm and a size distribution histogram over 30 measurements. (**C**) AuNSTs: TEM image of AuNSTs 26.0±2.6 nm, UV–VIS spectrum with a maximum at 630 nm and shoulder at 530 nm and a size distribution histogram over 30 measurements. (**D**) AuNFs: TEM image of AuNFs 40.6±2.2 nm, UV–VIS spectrum with a maximum at 563 nm and a size distribution histogram over 30 measurements (excluding the small spheres).
Abbreviations: AuNS, gold nanosphere; TEM, transmission electron microscopy; UV, ultraviolet; VIS, visible; AuNST, gold nanostar; AuNF, gold nanoflower; au, arbitrary unit.

was used for its stable and nontoxic nature.[49] It acts as a structure-directing agent, causing the formation of multiple protrusions from a spherical core while also stabilizing the particles in solution. Characterization of the AuNSTs can be seen in Figure 1C. The mean diameter of the AuNSTs was 26.0±2.6 nm. The UV–VIS spectrum shows two clear peaks, at 338 nm and 630 nm, with a shoulder ~530 nm. The peak at 338 nm originates from unreacted gold ions, while the peaks at 530 and 630 nm represent the transverse and longitudinal plasmon peaks of the particles, respectively. The longitudinal peak is quite broad, which, as can be seen from the TEM image, indicates that the length of the protrusions varied to some extent for the particles.

AuNFs were initially prepared according to a method by Xie et al,[50] following a very similar procedure as for the AuNSTs but with a higher HEPES to Au^{3+} ratio. However, after multiple trials, no satisfactory reproduction was obtained and the particles had no distinct petal like protrusions. Thus, another method was investigated to reliably produce these AuNFs. Adaptation and optimization were performed using a method described by Maiorano et al,[47] which is, in contrast to the method by Xie et al, a seed-mediated method. The same AuNS seeds were used as previously described. A slow addition of a $HAuCl_4$ solution to a mixture of HEPES and a specific seed concentration ensured that the AuNF formation was in a similar size range as the other particles. The AuNFs were prepared at 4°C to avoid primary nucleation in the solution as much as possible. A typical TEM image can be seen in Figure 1D, as well as the size distribution and UV-VIS spectrum. In the TEM image, some small spherical particles can also be observed; these are the result of primary nucleation, since their diameter is too small to be unreacted AuNS seeds and were excluded from the size measurements and histogram. Together, the TEM image and size distribution show that the particles obtained were highly uniform in size and shape.

The main difference in shape between the AuNFs and AuNSTs was that the AuNFs possessed much smaller but more numerous protrusions, while the AuNSTs possessed ~4–6, generally longer protrusions. The UV–VIS spectrum of the AuNFs shows a peak at 326 and 563 nm. The peak at 326 nm is attributed to the unreacted gold ions. The peak at 563 nm is the surface plasmon resonance peak of the AuNFs. Owing to the small size of the protrusions, there was no additional longitudinal peak. This agrees with the observations by Maiorano et al,[47] in which only protrusions exceeding a certain aspect ratio caused the appearance of these additional peaks. However, the position of the peak is markedly red shifted by ~34 nm compared to AuNSs of the same diameter.[51] This can be explained in the context of plasmon hybridization theory,[52] which regards the AuNFs as a hybrid of spheres and branched or rod-shaped particles.[50,53] This results in a plasmon resonance peak position intermediate to that of spheres (~530 nm) and branched (~700 nm) particles. Comparing the shape and position of the longitudinal peak of the AuNSTs with that of the AuNFs shows that the protrusions are smaller for the AuNFs, as indicated by a blue shift of the peak position. Additionally, the peak of the AuNFs is narrower, indicating a more uniform protrusion size.

Zeta potential measurement of the particles redispersed in cell culture medium (DMEM) showed a slight negative charge on the particles: −4.52±0.66 mV, −7.55±0.73 mV and −14.88±0.66 mV for the AuNSs, AuNFs and AuNSTs, respectively. Values of −15 to −30 mV were observed by Maiorano et al[47] and by Xie et al[50] for similar HEPES-capped particles, where a reduction in surface charge can be expected due to protein absorption on the particle surfaces when suspended in the cell culture medium.

Antibacterial studies with *S. aureus*

All purified AuNPs were diluted into 3 wt% TSB to obtain 1, 5, 10, 50, 100, 500 and 1,000 µg/mL solutions. In 96-well plates, 100 µL of a *S. aureus* bacterial culture at 10^6 bacteria/mL was added to 100 µL of the NP solution. Absorbance measurements were recorded at 592 nm (OD_{592}) for 24 hours to evaluate the antibacterial effects of the NPs; the results can be seen in Figure 2A and B.

As seen in Figure 2, the addition of either 250 or 500 µg/mL of AuNSs does not cause an antibacterial effect but rather gives similar growth curves as the NP-free control. Both AuNSTs and AuNFs show a significant, dose-dependent, antibacterial effect at 250 and 500 µg/mL, indicated by a large increase in lag time and a significant decrease in exponential growth rate. Interestingly, for both the AuNSTs and AuNFs, an initial increase in OD was observed, with a decline after ~300 min. It is speculated here that the initial increase in OD was due to a complex formation as the NPs attach to the bacterial cell membranes. This increase is higher for the AuNFs because their increased surface area may allow them to more readily form complexes with the bacteria. The antibacterial mechanism may have similarities to that observed previously where nanostructured surfaces with a high-aspect ratio, spikes[30] and pillars,[31] induced high local stress on the bacteria membrane inducing membrane rupture. Ultimately, this interaction kills the bacteria, causing a drop in OD, as observed. This process causes an overall decrease in exponential growth rate and an increase in lag time.

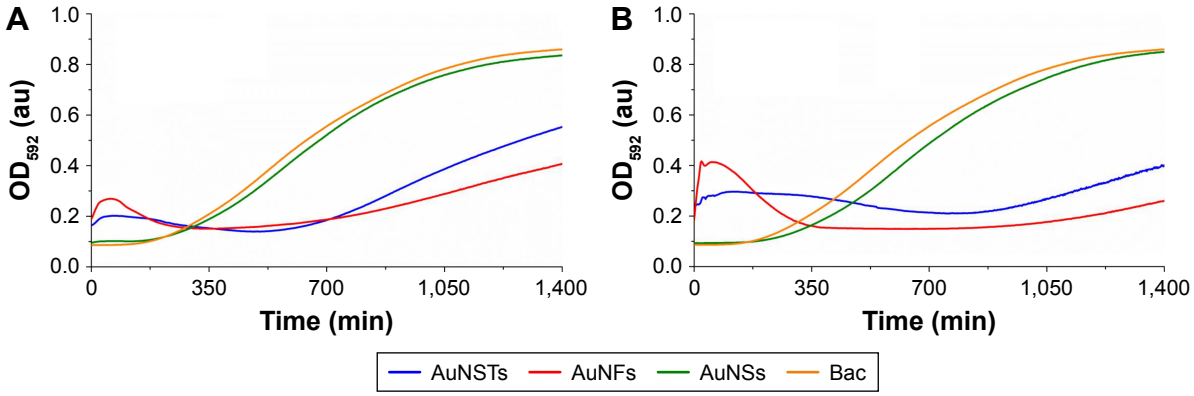

Figure 2 Bacterial growth curves (N=3).
Notes: Addition of (**A**) 250 µg/mL and (**B**) 500 µg/mL of AuNSTs, AuNFs and AuNSs to *S. aureus*. OD_{592} measured for 24 h at 2-minute intervals, mean values plotted. The control with only bacteria is denoted as Bac.
Abbreviations: AuNST, gold nanostar; AuNF, gold nanoflower; AuNS, gold nanosphere; *S. aureus*, *Staphylococcus aureus*; OD_{592}, optical density measured at 592 nm; au, arbitrary unit.

Further experiments are necessary to validate this possible mechanism.

Quantification of the antibacterial effect was achieved by fitting the absorbance growth curves to a parameterized Gompertz model as described by Zwietering et al,[45] which gives the following equation:

$$y = A \exp\left\{-\exp\left[\frac{\mu_m e}{A}(\lambda - t) + 1\right]\right\}$$

in which y is defined as the absorbance, A as the asymptotic absorbance, μ_m as the exponential growth rate, λ as the lag time, and t as the time in minutes. The optimum values for these three constants (A, μ_m, and λ) were found by minimizing the sum of least squares. The lag time is defined as the time at which an extrapolation of the tangent through the inflection point crosses y=0. In general, a very high correlation was found for all conditions with R^2=0.99–0.9999. The effect of the differently shaped AuNPs on the lag time can be seen in Figure 3, and the effect on the exponential growth rate is shown in Figure 4.

As can be seen in Figure 3, the addition of NPs caused a significant increase in lag time; however, the increase in the AuNSs was relatively small. The addition of 250 µg/mL AuNFs did not have a significant effect, although this was borderline (P=0.064). For both AuNSTs and AuNFs, the increase in lag time was large, with increases in lag time up to 280 and 310%, respectively, upon the addition of 500 µg/mL. For AuNSTs, the lag time also increased significantly as the concentration doubled. However, due to the quite large error bar for the 250 µg/mL AuNFs, this could not be concluded for the AuNFs. Looking at the effect of the AuNPs on the exponential growth rate in Figure 4, it can be seen that the addition of AuNS did not elicit a significant effect on the growth rate of *S. aureus*. Both the AuNSTs and AuNFs caused a significant decrease in the exponential growth rate, ~59 and 76%, respectively, upon the addition of 500 µg/mL. For both, a significant concentration- and shape-dependent effect was observed. The AuNFs proved to be the most effective in reducing the growth rate of *S. aureus*. Since the change in shape shows a significant difference in the antibacterial effect, it may be speculated that this is due to the higher surface area and higher numbers of protrusions on the surface. This may allow the AuNFs to attach to the bacteria more readily[54] and subsequently rupture the membrane with the protrusions, inducing cell death and/or other cellular functions.

When evaluating the increased antibacterial efficacy of the AuNFs compared to the AuNSTs, another factor needs

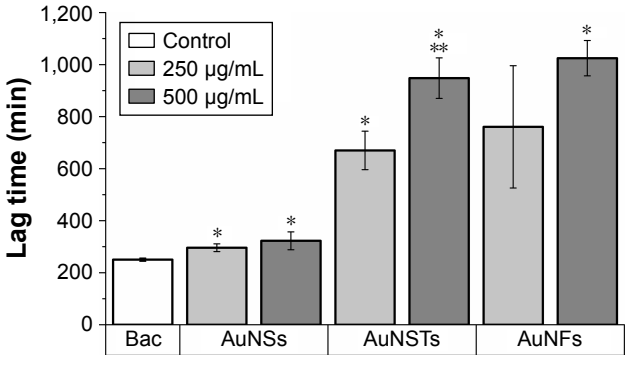

Figure 3 Lag time effect (N=3).
Notes: The significant (P<0.05) increase in lag time compared to the control is denoted by *. The significant increase compared to 250 µg/mL AuNSTs is denoted by **. The control with only bacteria is denoted as Bac.
Abbreviations: AuNST, gold nanostar; AuNS, gold nanosphere; AuNF, gold nanoflower.

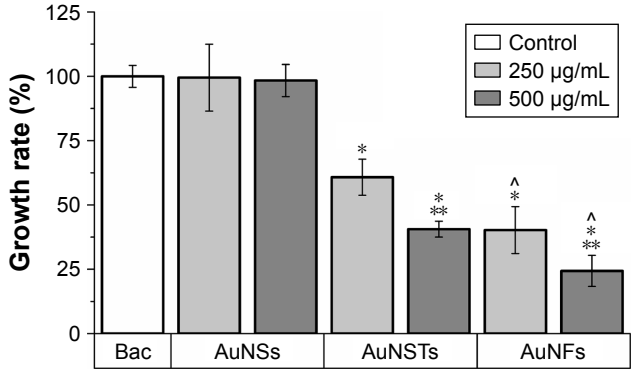

Figure 4 Exponential growth rate effect (N=3).
Notes: The significant ($P<0.05$) decrease in exponential growth rate compared to the control is denoted by *. The significant effect of increase in NP concentration is denoted by **. The significant effect of different shape is denoted by ^. The control with only bacteria is denoted as Bac.
Abbreviations: NP, nanoparticle; AuNS, gold nanosphere; AuNST, gold nanostar; AuNF, gold nanoflower.

to be taken into account. The bacteria were exposed to the same mass of the three different NPs during the assays; however, since there is a difference in shape and average size of the particles, the dosage calculated based on number is markedly different. Assuming the volume of the AuNSTs can be approximated by a sphere of 70% of their diameter (justification for this can be found in the Supplementary materials), this leads to up to 11 times fewer AuNFs than AuNSTs with the same mass dosage. The number-based antibacterial efficacy is therefore up to 11 times higher when comparing AuNFs to AuNSTs. Since the AuNSs have a size between the AuNSTs and the AuNFs and show no significant antibacterial effect, the AuNFs and AuNSTs efficacy may still be largely attributed to their shape and resulting surface area difference.

Cytotoxicity studies on HDFs

A significant effort was made to evaluate mammalian cell cytotoxicity of the differently shaped AuNPs in order to initially determine if the particles could be used safely. Cytotoxicity was evaluated by MTS assays and confocal microscopy. The viability of HDF cells following 4 days of culture with AuNPs can be seen in Figure 5A and B.

As can be seen in Figure 5, there was no significant cytotoxic effect observed via the MTS assays for any of the NPs. Moreover, a slight increase in viability was observed, even after correction for the increased absorption due to an increased amount of NPs present. Note that the highest concentration of NPs was 1,000 µg/mL, whereas 500 µg/mL was the highest concentration present with the bacteria. However, MTS assays could not give definitive evidence that the cells did not experience adverse effects due to the NPs. As observed by Pernodet et al,[35] even though MTS assay results may not indicate a cytotoxic effect, there can still be morphological and functional changes due to the addition of NPs.

To evaluate this further, confocal microscopy was performed on HDFs incubated with 25 and 500 µg/mL AuNPs for 4 days. These cells were stained with FITC–anti-vinculin (green), Alexa Fluor 568 phalloidin (red) and Hoechst 33258 (blue) to observe focal adhesion points, actin fibrils and cell nuclei, respectively. The results can be seen in Figure 6A–G.

Control HDF cells without the addition of NPs can be seen in Figure 6A. The cells displayed a normal, healthy morphology, and vinculin and actin were well expressed. Comparing this to the morphology of HDF treated with various concentrations and shapes of NPs, no morphological

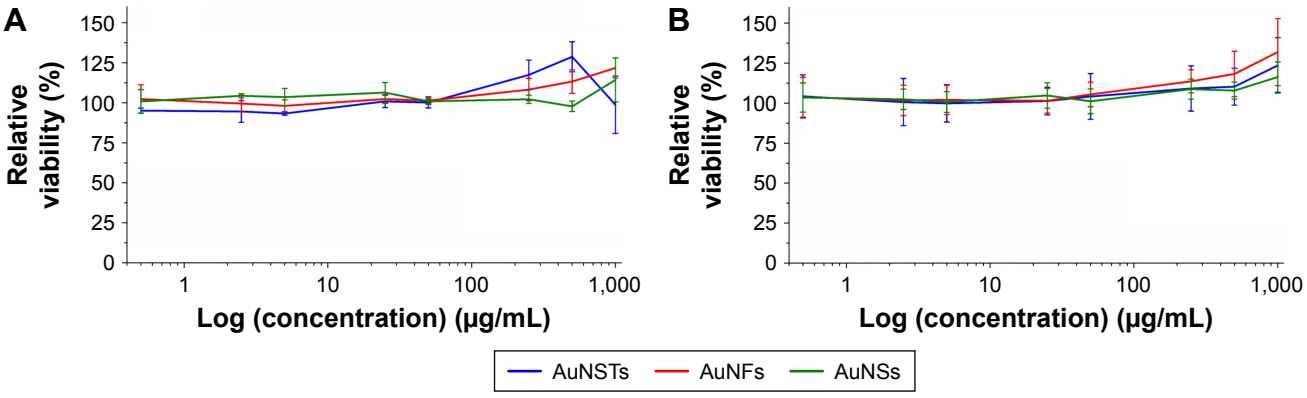

Figure 5 MTS assays (N=3).
Notes: Incubation of HDFs with AuNPs for 4 days. Cytotoxicity was evaluated by expressing the relative viability and by setting the viability of the cells incubated without NPs to 100%. (**A**) batch 1 and (**B**) batch 2.
Abbreviations: MTS, 3-(4,5 dimethylthiazol-2-yl)-5-(3-carboxymethoxyphenyl)-2-(4-sulfophenyl)-2H-tetrazolium; HDF, human dermal fibroblast; AuNP, gold nanoparticle; NP, nanoparticle; AuNS, gold nanosphere; AuNF, gold nanoflower; AuNST, gold nanostar.

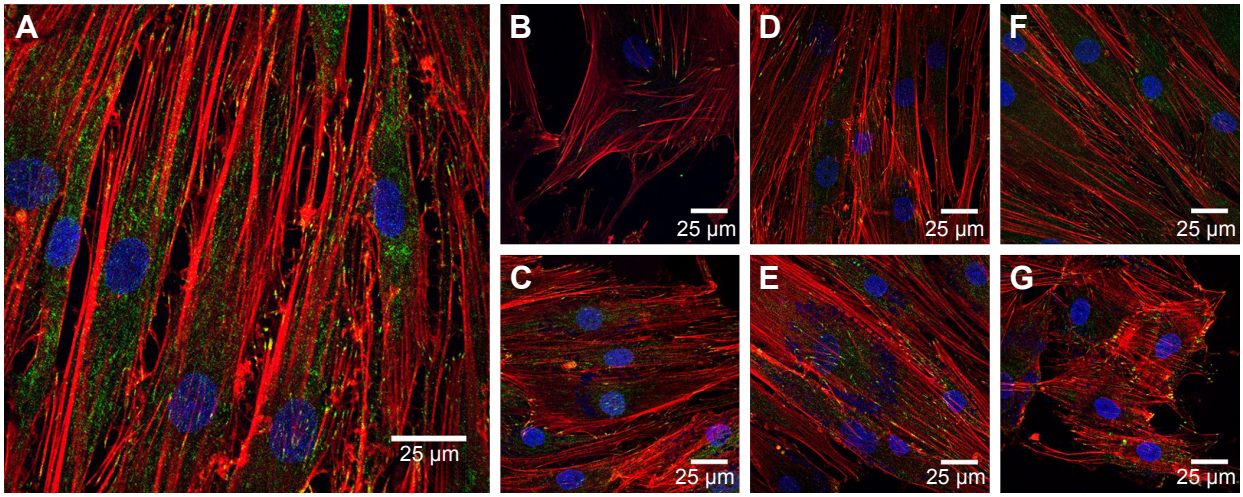

Figure 6 Confocal microscopy of HDFs.
Notes: Vinculin focal adhesion points were stained with FITC–anti-vinculin (green), actin fibrils were stained with Alexa Fluor 568 phalloidin (red) and cell nuclei were stained with Hoechst 33258 (blue). (**A**) Control without NPs, (**B**) 25 µg/mL AuNSTs, (**C**) 500 µg/mL AuNSTs, (**D**) 25 µg/mL AuNFs, (**E**) 500 µg/mL AuNFs, (**F**) 25 µg/mL AuNSs and (**G**) 500 µg/mL AuNSs. The NPs also appear in blue.
Abbreviations: HDF, human dermal fibroblast; FITC, fluorescein isothiocyanate; NP, nanoparticle; AuNST, gold nanostar; AuNF, gold nanoflower; AuNS, gold nanosphere.

changes were observed. Disruption of the actin fibrils as observed by Pernodet et al[35] after the addition of citrate-capped AuNSs was not present after the addition of any of the AuNPs prepared here. This indicates that in accordance with the MTS assays, the difference in the shape of the AuNPs studied here did not cause a cytotoxic effect on the HDF. This may be due to the chemical capping with the HEPES buffer, which is itself nontoxic. Interestingly, AuNP clusters can also be observed as blue dots at the same excitation wavelength used for the Hoechst dyes (352 nm). Although Hoechst dye has been previously used to stain DNA released into the cytoplasm from damaged cell nuclei,[55] that is not likely what was observed here as the MTS assays indicated that the metabolic activity of the cells was not affected. Additionally, the clusters are observed in a concentration-dependent manner and are absent in the control images without NPs.

To evaluate in more detail if the observed blue dots originated from NPs, trials were performed with the AuNSTs in 100 mM HEPES buffer and in DMEM with or without the addition of the Hoechst stain. The resulting confocal microscopy images can be seen in Figure S1A–D. Fluorescence upon excitation at 352 nm was observed for all samples containing the particles, indicating autofluorescence of the particles. Additionally, the fluorescence seems enhanced when the particles were in DMEM, which could be explained by agglomeration of the particles due to protein attachment. This protein corona formation would be enhanced further when the particles are incorporated into the cells after several days of incubation, as seen in Figure 6, and could further explain the very low cytotoxicity of the AuNPs as observed with the MTS assays.[56]

To evaluate the position of the AuNPs, either in or on the cells, confocal images were taken at different depths throughout the cells. Z-stack imaging for the 500 µg/mL addition of AuNFs can be seen in Figure 7. Similar results were obtained for all samples with the addition of AuNSs, AuNSTs and AuNFs at both 25 and 500 µg/mL concentrations. It can be clearly seen that a considerable amount of NPs were internalized within the cells and concentrated around the cell nucleus.

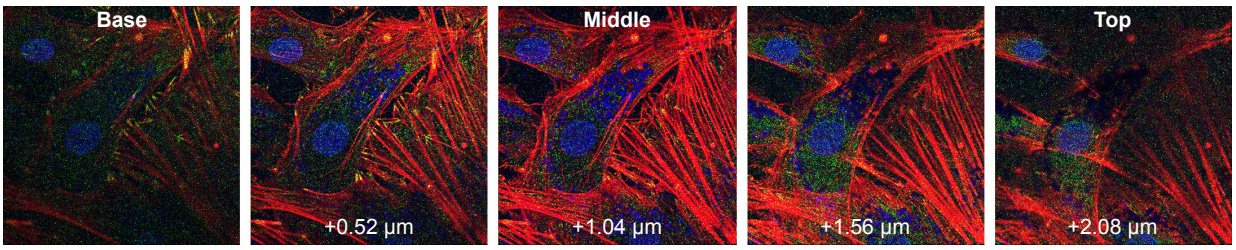

Figure 7 Confocal microscopy of HDFs.
Notes: Z-stack imaging of 500 µg/mL AuNFs with steps of 0.52 µm. Left to right from plate side to lumen.
Abbreviations: HDF, human dermal fibroblast; AuNF, gold nanoflower.

Conclusion

The synthesis of differently shaped AuNPs (specifically, AuNSs, AuNSTs and AuNFs) was achieved here with good uniformity, consistent surface chemistry and in a similar size range. HEPES buffer was used as a nontoxic dispersing agent to ensure a biocompatible Au surface chemistry.

Most interestingly, a shape-dependent antibacterial effect toward *S. aureus* was found via treatments over a broad concentration range from 0.5 to 500 μg/mL. Analysis of the growth curves obtained from 24 h optical density measurements showed a strong increase in lag time and a decrease in the exponential growth rate upon the addition of 250–500 μg/mL of AuNSTs and AuNFs. The AuNSs did not elicit any significant antibacterial effect toward *S. aureus*. Quantification and statistical analysis of the antibacterial effect were achieved by fitting data to a parameterized Gompertz model. Statistically significant increases in lag time for all shapes of particles were observed, with up to 3.8- and 4.1-fold increases in lag time upon the addition of 500 μg/mL AuNSTs and AuNFs, respectively. The exponential growth rate was not significantly affected by the addition of AuNSs, but showed a significant decrease – ~59 and 76% – upon the addition of 500 μg/mL AuNSTs and AuNFs, respectively.

Cytotoxicity of the AuNPs toward human cells was evaluated by incubating HDF with varying concentrations of the particles ranging from 0.5 to 1,000 μg/mL for 4 days. MTS viability assays and confocal microscopy showed neither reduction in viability of the cells at any concentration nor any changes in cell morphology. Using Z-stack imaging, it was shown that the AuNPs were internalized and concentrated in the area around the cell nucleus.

With no indications of a mammalian cell cytotoxic effect and a significant antibacterial effect, the present study provides the first evidence that AuNFs may be suitable candidates for use as a novel antibacterial agent (without resorting to the use of antibiotics). Long-term bacterial and mammalian cell exposure effects need to be further evaluated, including elucidation of the exact interactions between the particles and the cell membranes. The antibacterial efficacy could be further enhanced through selective targeting and radiative excitation to take advantage of the plasmon resonance effects of AuNPs.

Acknowledgment

The authors would like to thank Northeastern University for funding this research and W Fowle (Northeastern University) for his support with the TEM studies.

Disclosure

The authors report no conflicts of interest in this work.

References

1. Corma A, Garcia H. Supported gold nanoparticles as catalysts for organic reactions. *Chem Soc Rev*. 2008;37(9):2096–2126.
2. Homola J, Yee SS, Gauglitz G. Surface plasmon resonance sensors: review. *Sens Actuators B Chem*. 1999;54(1–2):3–15.
3. Turkevich J, Stevenson PC, Hillier J. A study of the nucleation and growth processes in the synthesis of colloidal gold. *Discuss Faraday Soc*. 1951;11:55–75.
4. Nikoobakht B, El-Sayed MA. Preparation and growth mechanism of gold nanorods (NRs) using seed-mediated growth method. *Chem Mater*. 2003;15(10):1957–1962.
5. Johnson CJ, Dujardin E, Davis SA, Murphy CJ, Mann S. Growth and form of gold nanorods prepared by seed-mediated, surfactant-directed synthesis. *J Mater Chem*. 2002;12(6):1765–1770.
6. Sun Y, Xia Y. Shape-controlled synthesis of gold and silver nanoparticles. *Science*. 2002;298(5601):2176–2179.
7. Xie J, Lee JY, Wang DIC. Seedless, surfactantless, high-yield synthesis of branched gold nanocrystals in HEPES buffer solution. *Chem Mater*. 2007;19(11):2823–2830.
8. Sperling RA, Rivera Gil P, Zhang F, Zanella M, Parak WJ. Biological applications of gold nanoparticles. *Chem Soc Rev*. 2008;37(9):1896–1908.
9. Pingarrón JM, Yáñez-Sedeño P, González-Cortés A. Gold nanoparticle-based electrochemical biosensors. *Electrochim Acta*. 2008;53(19):5848–5866.
10. Paciotti GF, Myer L, Weinreich D, et al. Colloidal gold: a novel nanoparticle vector for tumor directed drug delivery. *Drug Deliv*. 2004;11(3):169–183.
11. Boisselier E, Astruc D. Gold nanoparticles in nanomedicine: preparations, imaging, diagnostics, therapies and toxicity. *Chem Soc Rev*. 2009;38(6):1759–1782.
12. Huff TB, Tong L, Zhao Y, Hansen MN, Cheng J-X, Wei A. Hyperthermic effects of gold nanorods on tumor cells. *Nanomedicine (Lond)*. 2007;2(1):125–132.
13. Huang X, El-Sayed IH, Qian W, El-Sayed MA. Cancer cell imaging and photothermal therapy in the near-infrared region by using gold nanorods. *J Am Chem Soc*. 2006;128(6):2115–2120.
14. Zhang Y, Shareena Dasari TP, Deng H, Yu H. Antimicrobial activity of gold nanoparticles and ionic gold. *J Environ Sci Health C*. 2015;33(3):286–327.
15. Marambio-Jones C, Hoek EMV. A review of the antibacterial effects of silver nanomaterials and potential implications for human health and the environment. *J Nanopart Res*. 2010;12(5):1531–1551.
16. Zhou Y, Kong Y, Kundu S, Cirillo JD, Liang H. Antibacterial activities of gold and silver nanoparticles against *Escherichia coli* and bacillus Calmette-Guérin. *J Nanobiotechnology*. 2012;10(1):1–9.
17. Cui Y, Zhao Y, Tian Y, Zhang W, Lü X, Jiang X. The molecular mechanism of action of bactericidal gold nanoparticles on *Escherichia coli*. *Biomaterials*. 2012;33(7):2327–2333.
18. Li X, Robinson SM, Gupta A, et al. Functional gold nanoparticles as potent antimicrobial agents against multi-drug-resistant bacteria. *ACS Nano*. 2014;8(10):10682–10686.
19. Tom RT, Suryanarayanan V, Reddy PG, Baskaran S, Pradeep T. Ciprofloxacin-protected gold nanoparticles. *Langmuir*. 2004;20(5):1909–1914.
20. Grace AN, Pandian K. Quinolone antibiotic-capped gold nanoparticles and their antibacterial efficacy against gram positive and gram negative organisms. *J Bionanosci*. 2007;1(2):96–105.
21. Ahangari A, Salouti M, Heidari Z, Kazemizadeh AR, Safari AA. Development of gentamicin-gold nanospheres for antimicrobial drug delivery to staphylococcal infected foci. *Drug Deliv*. 2013;20(1):34–39.
22. Kalita S, Kandimalla R, Sharma KK, Kataki AC, Deka M, Kotoky J. Amoxicillin functionalized gold nanoparticles reverts MRSA resistance. *Mater Sci Eng C*. 2016;61:720–727.
23. Oleksiy F, Cholakov I, Borges M. *Antimicrobial Resistance Global Report on Surveillance*. Geneva: World Health Organization; 2014.
24. Klevens R, Morrison MA, Nadle J, et al; Active Bacterial Core surveillance (ABCs) MRSA Investigators. Invasive methicillin-resistant *Staphylococcus aureus* infections in the United States. *JAMA*. 2007;298(15):1763–1771.

25. Kishii K, Ito T, Watanabe S, Okuzumi K, Hiramatsu K. Recurrence of heterogeneous methicillin-resistant *Staphylococcus aureus* (MRSA) among the MRSA clinical isolates in a Japanese university hospital. *J Antimicrob Chemother*. 2008;62(2):324–328.
26. Millenbaugh N, Baskin J, DeSilva M, Elliott WR, Glickman R. Photothermal killing of *Staphylococcus aureus* using antibody-targeted gold nanoparticles. *Int J Nanomedicine*. 2015;10:1953–1960.
27. Simon-Deckers A, Brun E, Gouget B, Carrière M, Sicard-Roselli C. Impact of gold nanoparticles combined to X-Ray irradiation on bacteria. *Gold Bull*. 2008;41(2):187–194.
28. Hasan J, Crawford RJ, Ivanova EP. Antibacterial surfaces: the quest for a new generation of biomaterials. *Trends Biotechnol*. 2013;31(5):295–304.
29. Bazaka K, Crawford RJ, Ivanova EP. Do bacteria differentiate between degrees of nanoscale surface roughness? *Biotechnol J*. 2011;6(9):1103–1114.
30. Sjöström T, Nobbs AH, Su B. Bactericidal nanospike surfaces via thermal oxidation of Ti alloy substrates. *Mater Lett*. 2016;167:22–26.
31. Pogodin S, Hasan J, Baulin Vladimir A, et al. Biophysical model of bacterial cell interactions with nanopatterned cicada wing surfaces. *Biophys J*. 2013;104(4):835–840.
32. Chaurasia AK, Thorat ND, Tandon A, Kim J-H, Park SH, Kim KK. Coupling of radiofrequency with magnetic nanoparticles treatment as an alternative physical antibacterial strategy against multiple drug resistant bacteria. *Sci Rep*. 2016;6:33662.
33. Zhao Y, Ye C, Liu W, Chen R, Jiang X. Tuning the composition of AuPt bimetallic nanoparticles for antibacterial application. *Angew Chem Int Ed*. 2014;53(31):8127–8131.
34. Favi PM, Valencia MM, Elliott PR, et al. Shape and surface chemistry effects on the cytotoxicity and cellular uptake of metallic nanorods and nanospheres. *J Biomed Mater Res A*. 2015;103(12):3940–3955.
35. Pernodet N, Fang X, Sun Y, et al. Adverse effects of citrate/gold nanoparticles on human dermal fibroblasts. *Small*. 2006;2(6):766–773.
36. Katsumiti A, Arostegui I, Oron M, Gilliland D, Valsami-Jones E, Cajaraville MP. Cytotoxicity of Au, ZnO and SiO2 NPs using in vitro assays with mussel hemocytes and gill cells: relevance of size, shape and additives. *Nanotoxicology*. 2016;10(2):185–193.
37. Chithrani BD, Ghazani AA, Chan WCW. Determining the size and shape dependence of gold nanoparticle uptake into mammalian cells. *Nano Lett*. 2006;6(4):662–668.
38. Pan Y, Neuss S, Leifert A, et al. Size-dependent cytotoxicity of gold nanoparticles. *Small*. 2007;3(11):1941–1949.
39. Favi PM, Gao M, Johana Sepúlveda Arango L, et al. Shape and surface effects on the cytotoxicity of nanoparticles: gold nanospheres versus gold nanostars. *J Biomed Mater Res A*. 2015;103(11):3449–3462.
40. Albanese A, Tang PS, Chan WCW. The effect of nanoparticle size, shape, and surface chemistry on biological systems. *Annu Rev Biomed Eng*. 2012;14(1):1–16.
41. Goodman C, McCusker C, Yilmaz T, Rotello V. Toxicity of gold nanoparticles functionalized with cationic and anionic side chains. *Bioconjug Chem*. 2004;15(4):897–900.
42. Chu Z, Zhang S, Zhang B, et al. Unambiguous observation of shape effects on cellular fate of nanoparticles. *Sci Rep*. 2014;4:4495.
43. Arnida, Malugin A, Ghandehari H. Cellular uptake and toxicity of gold nanoparticles in prostate cancer cells: a comparative study of rods and spheres. *J Appl Toxicol*. 2010;30(3):212–217.
44. Wang S, Lawson R, Ray PC, Yu H. Toxic effects of gold nanoparticles on *Salmonella typhimurium* bacteria. *Toxicol Ind Health*. 2011;27(6):547–554.
45. Zwietering MH, Jongenburger I, Rombouts FM, van 't Riet K. Modeling of the bacterial growth curve. *Appl Environ Microbiol*. 1990;56(6):1875–1881.
46. Park Y-K, Park S. Directing close-packing of midnanosized gold nanoparticles at a water/hexane interface. *Chem Mater*. 2008;20(6):2388–2393.
47. Maiorano G, Rizzello L, Malvindi MA, et al. Monodispersed and size-controlled multibranched gold nanoparticles with nanoscale tuning of surface morphology. *Nanoscale*. 2011;3(5):2227–2232.
48. Smoluchowski MV. Drei Vortrage uber Diffusion. Brownsche Bewegung und Koagulation von Kolloidteilchen. [Three lectures on diffusion, Brownian motion and coagulation of colloid particles]. *Z Phys*. 1916;17:557–585. German.
49. Good NE, Winget GD, Winter W, Connolly TN, Izawa S, Singh RMM. Hydrogen ion buffers for biological research. *Biochemistry*. 1966;5(2):467–477.
50. Xie J, Zhang Q, Lee JY, Wang DIC. The synthesis of SERS-active gold nanoflower tags for in vivo applications. *ACS Nano*. 2008;2(12):2473–2480.
51. Joseph V, Matschulat A, Polte J, Rolf S, Emmerling F, Kneipp J. SERS enhancement of gold nanospheres of defined size. *J Raman Spectrosc*. 2011;42(9):1736–1742.
52. Prodan E, Radloff C, Halas NJ, Nordlander P. A hybridization model for the plasmon response of complex nanostructures. *Science*. 2003;302(5644):419–422.
53. Hao E, Bailey RC, Schatz GC, Hupp JT, Li S. Synthesis and optical properties of "branched" gold nanocrystals. *Nano Lett*. 2004;4(2):327–330.
54. Shamaila S, Zafar N, Riaz S, Sharif R, Nazir J, Naseem S. Gold nanoparticles: an efficient antimicrobial agent against enteric bacterial human pathogen. *Nanomaterials*. 2016;6(4):71.
55. Belloc F, Dumain P, Boisseau MR, et al. A flow cytometric method using Hoechst 33342 and propidium iodide for simultaneous cell cycle analysis and apoptosis determination in unfixed cells. *Cytometry*. 1994;17(1):59–65.
56. Tenzer S, Docter D, Kuharev J, et al. Rapid formation of plasma protein corona critically affects nanoparticle pathophysiology. *Nat Nanotechnol*. 2013;8(10):772–781.

Supplementary materials

Justification for calculation of the mass to number equivalency of the gold nanostars (AuNSTs) versus the gold nanoflowers (AuNFs)

The AuNSTs of a diameter of 26±2.6 nm have approximately the same volume as a sphere with 70% that diameter (18.2 nm). The 70% is justified since the AuNSTs, as measured from the transmission electron microscopy (TEM) images, have a core diameter of ~18 nm with, on average, five protrusions of 5 by 8 nm (diameter by height) which leads (assuming conical protrusions) to a volume of 2.55×10^{-5} μm^3 per particle. This is the same volume as a sphere with approximately 70% of the total diameter (2.53×10^{-5} μm^3 per particle). The volume of the AuNFs can be approximated by a sphere of the same diameter, since the protrusions are so small (and so numerous) compared to the diameter, thus leading to a volume of 2.80×10^{-4} μm^3 per particle. Using the density of gold (19.3 g/cm^3), this results in 2.05×10^{15} AuNSTs per gram and 1.85×10^{14} AuNFs per gram. The number ratio between the AuNSTs and AuNFs can then be calculated by dividing the number of particles per gram for each particle shape, resulting in 11.08. This means 11.08 times more AuNSTs per gram than AuNFs. Note that the ratio of the volumes will give the same value, since the density for both particles is the same.

Confocal microscopy images of the evaluation of the auto-fluorescence of the AuNSTs in water or Dulbecco's Modified Eagle's Medium (DMEM), with or without the Hoechst stain

To confirm if the blue dots/clusters observed in the confocal images (Figures 6 and 7) were the AuNPs, trials were performed with the AuNSTs in 100 mM 4-(2-hydroxyethyl) piperazine-1-ethanesulfonic acid (HEPES) buffer and DMEM cell media with or without Hoechst 33258. The results of this can be seen in Figure S1A–D. In all images, some degree of fluorescence was observed, which indicates that autofluorescence of the AuNSTs occurred when excited with a 352 nm laser. The presence of the Hoechst stain did not seem to increase the amount of fluorescence. However, the fluorescence increased when the particles were in DMEM, most likely due to agglomeration of the particles in the presence of and due to protein adsorption.

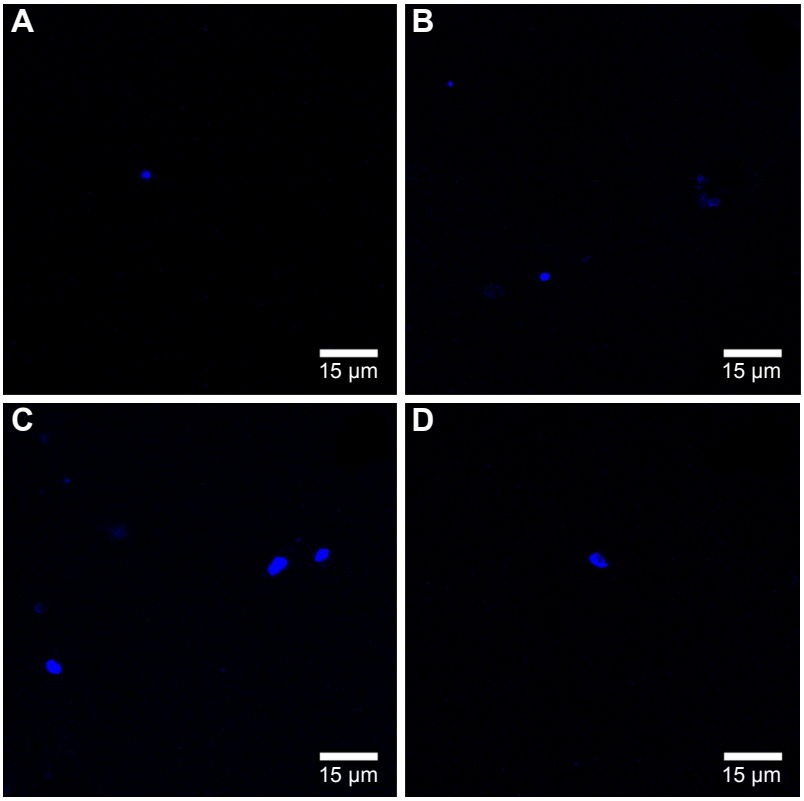

Figure S1 Confocal microscopy images of the evaluation of the auto-fluorescence of the AuNSTs in water or DMEM, with or without the Hoechst stain.
Notes: Confocal microscopy images with 352 nm laser excitation of AuNSTs clusters (**A**) in HEPES buffer, (**B**) in HEPES buffer with Hoechst 33258, (**C**) in DMEM and (**D**) in DMEM with Hoechst 33258.
Abbreviations: AuNST, gold nanostar; AuNF, gold nanoflower; HEPES, 4-(2-hydroxyethyl)piperazine-1-ethanesulfonic acid; DMEM, Dulbecco's Modified Eagle's Medium.

Calculation showing the comparison of approximate surface area AuNSTs to AuNFs

As stated earlier and under "Justification for calculation of the mass to number equivalency of the gold nanostars (AuNSTs) versus the gold nanoflowers (AuNFs)", the AuNSTs can be approximated by a sphere of 18 nm in diameter with, on average, five cone shaped protrusions of 5 by 8 nm (diameter by height). This will give an approximate surface area of 1.25×10^{-3} μm^2 per particle:

$$SA_{AuNST} = SA_{sphere} - n_{cones} * SA_{cone\ base} + n_{cones}(SA_{cone} - SA_{cone\ base}) = 1.25\times10^{-3}\ \mu m^2.$$

where $SA_{sphere} = 1.02\times10^{-3}$ μm^2, $n_{cones} = 5$, $SA_{cone\ base} = 1.96\times10^{-5}$ μm^2, and $SA_{cone} = 8.55\times10^{-5}$ μm^2.

For the AuNFs, it is impossible to accurately estimate the number of protrusions from TEM images, therefore, we assume here that the surface is evenly covered with cone-like protrusions of around 4 by 5 nm (diameter by height). Given the average diameter of the AuNFs is 40 nm, this gives a spherical core of 30 nm. To calculate the number of protrusions on the surface, the surface area of a 30 nm cone is divided by the cone base surface area with a diameter of 4 nm, corrected for the hexagonal packing parameter:

$$\eta_h = \frac{\pi}{2\sqrt{3}} \approx 0.9069$$

This gives:

$$SA_{AuNF} = SA_{sphere} - n_{cones} * SA_{cone\ base} + n_{cones}(SA_{cone} - SA_{cone\ base}) = 7.17\times10^{-3}\ \mu m^2.$$

where $SA_{sphere} = 2.83\times10^{-3}$ μm^2, $n_{cones} = \frac{SA_{sphere} * \eta_h}{SA_{cone\ base}} = 204$, $SA_{cone\ base} = 1.26\times10^{-5}$ μm^2, and $SA_{cone} = 4.64\times10^{-5}$ μm^2.

This results in a 5.74 times greater surface area for the AuNFs, on average, compared to the AuNSTs. When varying the number of AuNST protrusion by ±1 and the AuNF protrusion dimensions by ±1 nm, the surface area ratio varies between 4.5 and 7.5 times greater for the AuNFs.